

Charge Transport Properties of a Series of Metal Quinolates Utilising Dispersion-Corrected Density Functional Theory

Md. Rakib Hossain, Ahsan Ullah and Nazia Chawdhury*

Department of Physics, Shahjalal University of Science and Technology, Sylhet 3114, Bangladesh

*Correspondence E-mail: nc-phy@sust.edu

Published online: 28 April 2023

To cite this article: Hossain, M. R. et al. (2023). Charge transport properties of a series of metal quinolates utilising dispersion-corrected density functional theory. *J. Phys. Sci.*, 34(1), 75–85. <https://doi.org/10.21315/jps2023.34.1.7>

To link to this article: <https://doi.org/10.21315/jps2023.34.1.7>

ABSTRACT: *The electronic and charge transport properties of Metal-Quinolates (Metal = Li, Na, K, Rb and Cs) compounds are theoretically investigated using Austin-Frisch-Petersson functional with dispersion (APFD) corrected density functional theory (DFT). The calculated energy gap between highest occupied molecular orbital and lowest unoccupied molecular orbital ranges from 3.40 eV for LiQ to 0.93 eV for CsQ. The ionisation potential, electron affinity and chemical hardness of the compounds are calculated. We found that the electron hopping rate, $k_{electron}$ of CsQ is around 150 times greater than LiQ. We suggest that CsQ is the most efficient charge injecting or transport material for organic light-emitting diodes (OLEDs). Dimer formation is desirable with all M-Quinolate with different electronic structures and (CsQ)₂ dimer shows the lowest dimerisation energy.*

Keywords: *metal quinolate, charge transport, density functional theory*

1. INTRODUCTION

Organic light-emitting diodes (OLEDs) attracted tremendous attention after first reported by Tang et al. in 1987.^{1,2} OLEDs have been commercialised extensively because of their great potential for applications in flexible displays, solid-state lighting etc.^{3,4} Many studies have been carried out in order to enhance device performance in terms of material characteristics. The charge transport property of organic molecules is one of the most significant features to understand physical properties of organic electronic devices.^{5,6}

Recently, many researches have performed experiments using lithium-quinolate complexes such as 8-hydroxy-quinolinato lithium (LiQ) as an electron transporting layer (ETL) as well as an electron injection layer (EIL) in the OLED devices.^{7–11} LiQ has been the most widely utilised quinolate material.¹² The purpose of LiQ as an EIL is to reduce the energy barrier between the cathode and the ETL, allowing electrons injected from the cathode to be effectively transported through the ETL. But, because of poor electron carrier mobility, the LiQ can disrupt effective electron hopping in the ETL.¹³

To overcome poor electron mobility, as an alternative to LiQ, Jeon et al. recently has used the most famous hybrid density functional theory (DFT), B3LYP which stands for Becke, 3-parameter, Lee–Yang–Parr, for theoretical investigation of a series of Metal-Quinolate complexes (Metal = singly oxidised metal ions) to explain the influence of metal ions on electronic, and charge transport characteristics.¹⁴ However, the B3LYP functional does not account for the influence of van der Waals interactions with extended range, which are prevalent in nature. This research evaluates the electrical characteristics of a range of metal quinolate complexes using dispersion-corrected density functional theory. Austin-Frisch-Petersson functional with dispersion (APFD) is a hybrid functional that modifies the regular Austin-Frisch-Petersson functional by including dispersion adjustments.¹⁵ APFD provides significantly superior performance for a selection of compounds compared to B3LYP.^{16,17}

2. METHODOLOGY

For Metal-Quinolate materials (Metal = Li, Na, K, Rb, and Cs), the DFT simulations are carried out using unrestricted APFD with LanL2MB level of theory which is implemented in the suite of Gaussian 16 programme.¹⁸ The calculations are performed considering that both case of non-relativistic and relativistic effects. At the molecular level, the charge transport rate are derived by well-known Marcus's formalism.¹⁹

$$k_{\text{electron/hole}} = \frac{4\pi^2}{h} \frac{1}{\sqrt{4\pi\lambda_{e/h}k_B T}} J_{e/h}^2 e^{-\left[\frac{\lambda_{e/h}}{4k_B T}\right]} \quad (1)$$

where, h is the Planck's constant, k_B is the Boltzmann constant, T is the temperature, $\lambda_{e/h}$ is the reorganisation energy for electron or hole and $J_{e/h}$ is the charge transfer integral for electron or hole.

The charge transfer integral for the electron (J_e) and hole (J_h) have approximated from Koopmans' theory with equation (2).²⁰

$$J_e = \frac{(\text{LUMO} + 1) - \text{LUMO}}{2}, J_h = \frac{\text{HOMO} - (\text{HOMO} - 1)}{2}, \quad (2)$$

The reorganisation energy is considered as an essential parameter to comprehend the charge transport property. The inner reorganisation energies for hole and electron can be estimated by the addition of relaxation energies (λ_1 and λ_2 in Figure 1) under a reversible charge transition reaction.²¹

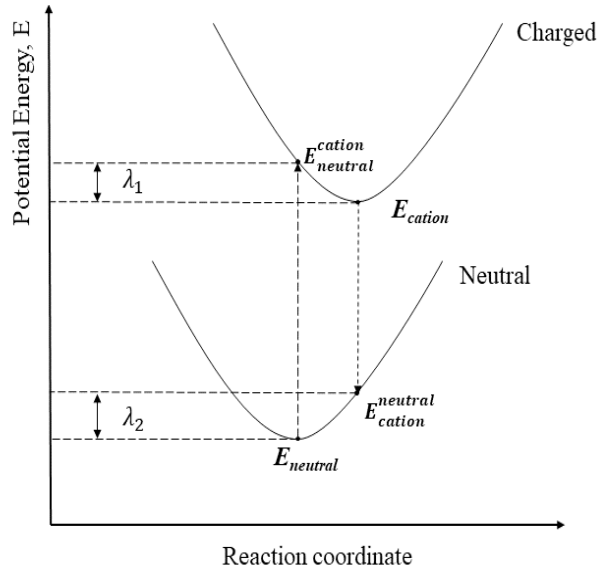


Figure 1: Potential energy curve for neutral and cationic structure.

The equations for λ_h and λ_e can be defined as:

$$\lambda_h = (E_{neutral}^{cation} - E_{cation}) + (E_{cation}^{neutral} - E_{neutral}) \quad (3)$$

$$\lambda_e = (E_{neutral}^{anion} - E_{anion}) + (E_{anion}^{neutral} - E_{neutral}) \quad (4)$$

3. RESULTS AND DISCUSSION

3.1 Optimised Geometries

The DFT/Unrestricted Austin-Frisch-Petersson Functional with Dispersion (UAPFD) molecular structures of Metal-Quinolates (Metal = Li, Na, K, Rb and Cs) are shown in Figure 2. Based on the singly oxidised metal ions, structural differences are found. The bond

This noticeable difference of electron density in HOMO and LUMO is predominantly described as charge transfer characteristic, known as ligand-to-metal charge transfer (LMCT).^{22,23} However, in LiQ we observe, ligand to ligand charge transfer character or $\pi-\pi^*$ with small contribution from lithium atom. We observe that the area around the aromatic carbon atom and the oxygen atom has a negative electrostatic potential and that of the metal has a positive electrostatic potential. While the atomic number of the metal ion increases, the electrostatic potential of the nucleophilic band increases and the electrophilic region decreases.

3.3 Electronic Energy Levels

The materials with lower band gap offers greater potential in electrical devices due to their inherent conductivity. Therefore, controlling the band gap is very crucial. The HOMO and LUMO energy levels, and the estimated energy difference between the HOMO and LUMO are shown in Figure 4. These results show that the energy gap (E_g) gradually decreases regarding to the increase of the atomic number of metal ions.

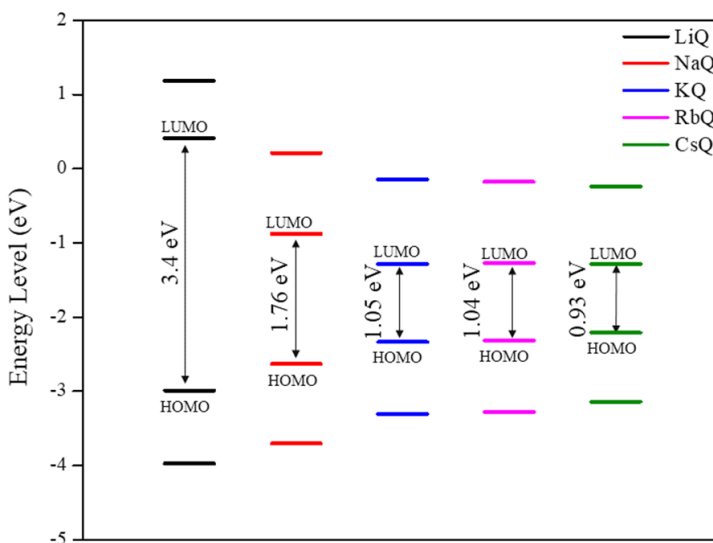


Figure 4: The HOMO and LUMO energy levels of LiQ, NaQ, KQ, RbQ and CsQ.

The energy gap is higher for LiQ and lower for CsQ amongst all the five molecules. Yadav et al. showed that for high charge recombination, the energy gap must be lower as the LUMO levels contribute in the recombination compared to HOMO levels, in organic layers.²⁴ We found that the estimated LUMO energy levels of NaQ, KQ, RbQ and CsQ are more stable than LiQ.

3.4 Ionisation Potential, Electron Affinity and Chemical Hardness

The performance of optoelectronic devices relies on the balanced charge transfer and charge injection.²⁵ The electron affinity (EA) of an organic semiconductor is not only a measurement of electron transport but also a key parameter to determine the suitability to use in organic electroluminescent devices. Accurate EA values are necessary for developing the device architecture of OLEDs. EA is determined as the variance in total energy between the anionic and neutral molecules.²⁶ The ionisation potential, (IP) is very significant to design the structure of organic molecules for organic electronics. We have analysed IP, EA and chemical hardness to understand the electronic structure of the metal complexes. Our calculation shows that CsQ has the minimum IP and maximum EA (Figure 5).

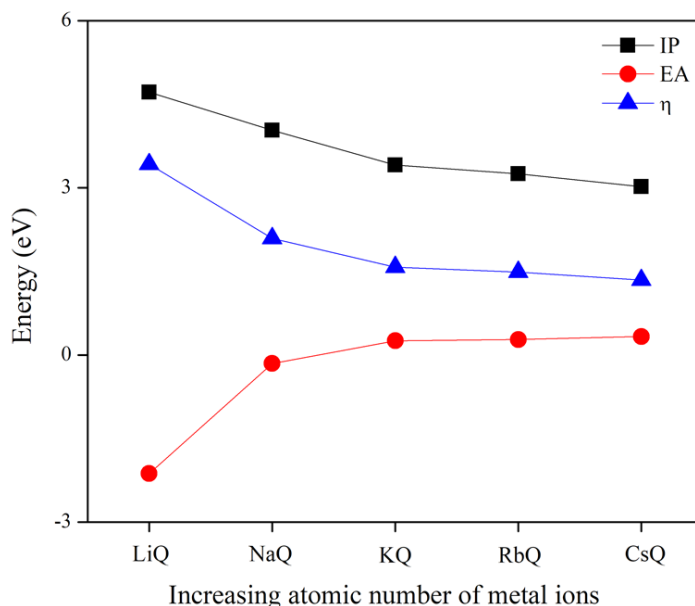


Figure 5: The IP, EA and chemical hardness (η) for LiQ, NaQ, KQ, RbQ and CsQ.

The trend of these calculated values is consistent with the calculation of Jeon et al.¹⁴ However, the theoretical results requires reasonable quantitative or qualitative comparison with the experimental reality. This will significantly increase the importance of this study. Figure 5 shows that the chemical hardness values follow the order $\text{LiQ} > \text{NaQ} > \text{KQ} > \text{RbQ} > \text{CsQ}$. This result suggests that CsQ is the most sensitive to redox reaction and therefore it is electrochemically reactive material to transport holes/electrons in OLEDs.

3.5 Charge Transfer Properties

Figure 6 shows the hole transport rate, k_{hole} and electron transport rate, k_{electron} of Metal-Quinolate complexes. We find that the calculated k_{hole} and k_{electron} values do not show a straightforward trend with increasing atomic number of metal ions. We note that the k_{electron} of CsQ is two orders of magnitudes higher than other quinolates in the series. To confirm the values of the charge transport rates, we have performed the calculations with LanL2MB basis set at unrestricted B3LYP level with Gaussian 16 using DFT method. We choose effective core potential (ECP) for reducing computational cost on systems with metal centers, and to describe relativistic effects in deep core electrons. LanL2MB includes both the basis set and ECP. Our calculations show quite similar as we observed applying unrestricted APFD with LanL2MB level.

At a given temperature, efficient charge transport needs a mechanism with low reorganisation energy and a high transfer integral. Koopmans' theorem provides a method for calculating the transfer integral, a measure of the strength of electronic coupling between adjacent molecules. CsQ shows the much lower reorganisation energy compared to all other investigated metal quinolates. However, the electron transfer integral of Metal-Quinolates is comparable. The charge transfer model suggests that the transfer rate of electrons and holes should predominate with their corresponding reorganisation energies of electron and hole, in the exponential term in equation (1).²⁷

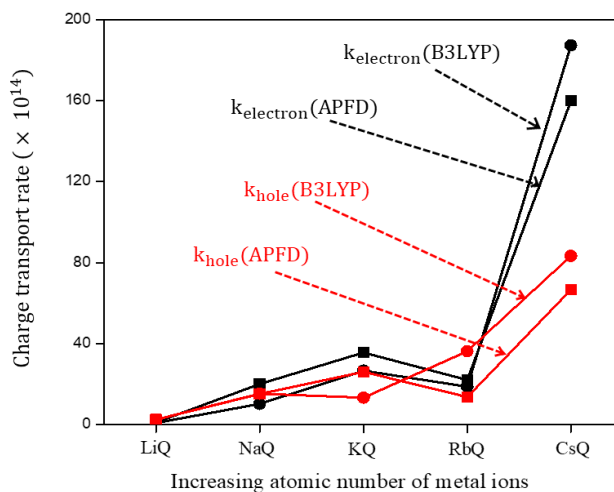


Figure 6: The intermolecular charge hopping rates of hole, k_{hole} and electron, k_{electron} of LiQ, NaQ, KQ, RbQ and CsQ calculated using two different functionals but with the same basis set.

Consequently, the electron transport rate in CsQ is higher than in other compounds. In addition, if the HOMO is less negative, electrons should be able to leave a hole transport material more readily. Nevertheless, it is anticipated that electrons are taken more easily by electron transport material with a lower LUMO value.²⁸ CsQ has the lowest LUMO value, indicating it to be a superior electron transport material. The HOMO and LUMO state distribution of Metal-Quinolates may be correlated to their charge transport characteristics. This is because the orbitals of different molecules will overlap more readily if the HOMO and LUMO are delocalised, allowing for more efficient hole/electron transport through hopping. A higher degree of localisation of the HOMO/LUMO states limits the hole/electron transport.²⁹ Though in CsQ HOMO/LUMO are not significantly delocalised, the trade of between delocalisation of HOMO/LUMO and the lower reorganisation energy, we conclude that CsQ shows much better electron transport property.

3.6 Dimerisation of Metal-Quinolates

Scanning Electron Microscope (SEM) studies on some synthesised metal quinolate complex crystals such as $\text{Co}(\text{8HQ})_2$ on glass substrate has detected those molecules aggregate from a single molecule to several molecules up to a size of several hundred nanometers.^{30, 31} Therefore, we are intrigued to study the dimerisation effects in these materials with considering the dispersion correction for van der Waals force.

The DFT/UAPFD molecular structures of Metal-Quinolate dimers are shown in Figure 7. It is observed that the optimised structure of $(\text{RbQ})_2$ and $(\text{CsQ})_2$ are very different from other calculated dimers. We see that by increasing the atomic number of metal ions, the benzene/quinol rings of two different molecules follow the trend to be oriented parallel to each other in the complex. Our result differs from the previous report of dimer formation by Jeon et al.¹⁴ This is the effect of changing functional and basis set. We recommend experimental verification for these results.

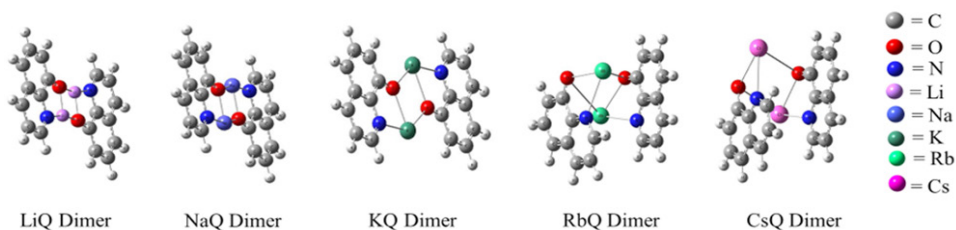


Figure 7: The basis set superposition error (BSSE) corrected optimised structures of Metal-Quinolate dimers, $(\text{LiQ})_2$, $(\text{NaQ})_2$, $(\text{KQ})_2$, $(\text{RbQ})_2$ and $(\text{CsQ})_2$.

The optimised dimeric structures show a variation of dimer formation for different metal ions. Structural bending for dimers occurs mostly at the bond angle of Metal-Oxygen-Carbon (MOC). While the atomic number of metal ions rises, the dihedral angle drops, and (RbQ)₂ and (CsQ)₂ display highly diverse optimal structures. The two types of significant bonds i.e., N-M and O-M are compared with monomer structure and found that the bond lengths in the dimeric structure are slightly higher than that of the monomer structure. The calculated dimerisation energy of CsQ shows the fragile binding strength amongst other quinolate complexes. BSSE corrected dimerisation energy is presented for all the dimers.

4. CONCLUSION

A series of Metal-Quinolate compounds with Metal = Li, Na, K, Rb and Cs are investigated theoretically in order to understand the effect of metal ions on electronic and charge transport properties by dispersion-corrected DFT. Our calculations do not show any significant variation while considering relativistic effects for the metal atoms in the complexes. The charge transfer integrals, the reorganisation energies, and also the intermolecular charge hopping rates are thoroughly presented to analyse charge transport properties. The significantly higher value of k_{electron} of CsQ compared to LiQ, NaQ, KQ and RbQ suggests that CsQ can act as an ETL in OLEDs. Dimer formation is desirable with all Metal-Quinolate. These results strongly suggest that CsQ shows finest characteristics in all perspective for acting as EIL and enhancer for ETL, consequently leading to high power and current efficiency of OLEDs. However, further work is required to show experimental correlation with the calculation performed with AFPD method.

5. ACKNOWLEDGEMENTS

We are grateful to Ministry of Education, Government of the People's Republic of Bangladesh (ID: PS2017535) and Ministry of Science and Technology, Bangladesh (ID: EAS 501) for financial support.

6. REFERENCES

1. Tang, C. W. & VanSlyke, S. A. (1987). Organic electroluminescent diodes. *Appl. Phys. Lett.*, 51, 913–915. <https://doi.org/10.1063/1.98799>
2. Chien, C. H. et al. (2009). Multifunctional deep-blue emitter comprising an anthracene core and terminal triphenylphosphine oxide groups. *Adv. Funct. Mater.*, 19, 560–566. <https://doi.org/10.1002/adfm.200801240>

3. Kang, S. et al. (2019). Unveiling the root cause of the efficiency-lifetime trade-off in blue fluorescent organic light-emitting diodes. *Electron. Mater. Lett.*, 16, 1–8. <https://doi.org/10.1007/s13391-019-00180-5>
4. Van Slyke, S. A. et al. (1996). Organic electroluminescent devices with improved stability. *Appl. Phys. Lett.*, 69, 2160–2162. <https://doi.org/10.1063/1.117151>
5. Rohloff, R. et al. (2017). Electron and hole transport in the organic small molecule α -NPD. *Appl. Phys. Lett.*, 110, 073301. <https://doi.org/10.1063/1.4976205>
6. Kang, S. et al. (2019). Design of efficient non-doped blue emitters: Toward the improvement of charge transport. *RSC Adv.*, 9, 27807–27816. <https://doi.org/10.1039/c9ra04918e>
7. Singh, D. et al. (2016). Optoelectronic properties of color-tunable mixed ligand-based light-emitting zinc complexes. *J. Elec. Mater.*, 45, 4865–4874. <https://doi.org/10.1007/s11664-016-4721-0>
8. Ki, M. S. et al. (2022). Improved thermal stability and operational lifetime of blue fluorescent organic light-emitting diodes by using a mixed-electron transporting layer. *ACS Mater. Lett.*, 4(9), 1676–1683. <https://doi.org/10.1021/acsmaterialslett.2c00583>
9. Schmitz, C. et al. (2000). Lithium–Quinolate complexes as emitter and interface materials in organic light-emitting diodes. *Chem. Mater.*, 12, 3012–3019. <https://doi.org/10.1021/cm0010248>
10. Zhou, D. Y. et al. (2010). Efficiency dependence on alkali metal compound/Al bilayer cathode in organic light-emitting diodes. *Appl. Phys. Lett.*, 97, 223302. <https://doi.org/10.1063/1.3522883>
11. Zheng, X. et al. (2005). Efficiency improvement of organic light-emitting diodes using 8-hydroxy-quinolinato lithium as an electron injection layer. *Thin Solid Films*, 478, 252–255. <https://doi.org/10.1016/j.tsf.2004.08.020>
12. Lee, W. & Jung, J. W. (2016). High performance polymer solar cells employing a low-temperature solution-processed organic–inorganic hybrid electron transport layer. *J. Mater. Chem. A*, 4, 16612–16618. <https://doi.org/10.1039/c6ta06911h>
13. Kim, J. H. & Park, J. W. (2017). Designing an electron-transport layer for highly efficient, reliable, and solution-processed organic light-emitting diodes. *J. Mater. Chem. C*, 5, 3097–3106. <https://doi.org/10.1039/c7tc00488e>
14. Jeon, S. H. et al. (2019). Discovering new M-quinolate materials: Theoretical insight into understanding the charge transport, electronic, self-aggregation properties in M-quinolate materials (M=Li, Na, K, Rb, Cs, Cu, Ag, and Au). *J. Mater. Sci.*, 54, 9523–9532. <https://doi.org/10.1007/s10853-019-03584-8>
15. Austin, A. et al. (2012). A density functional with spherical atom dispersion terms. *J. Chem. Theory Comput.*, 8, 4989–5007. <https://doi.org/10.1021/ct300778e>
16. Malloum, A. et al. (2018). Solvation energies of the proton in methanol revisited and temperature effects. *Phys. Chem. Chem. Phys.*, 20, 29184–29206. <https://doi.org/10.1039/c8cp05823g>
17. Hansen, P. E. et al. (2020). One-bond 1J (15 N,H) coupling constants at sp^2 -hybridized nitrogen of Schiff bases, enamines and similar compounds: A theoretical study. *Magn. Reson. Chem.*, 58, 750–762. <https://doi.org/10.1002/mrc.5052>

18. Frisch, M. J. E. A. et al. (2009). *Gaussian 09*. Wallingford: Gaussian. Inc. Marcus, R. A. & Sutin, N. (1985). Electron transfers in chemistry and biology. *Biochim. Biophys. Acta. Bioenerg.*, 811(3), 265–322. [https://doi.org/10.1016/0304-4173\(85\)90014-x](https://doi.org/10.1016/0304-4173(85)90014-x)
19. Marcus, R. A. & Sutin, N. (1985). Electron transfers in chemistry and biology. *Biochim. Biophys. Acta. Bioenerg.*, 811(3), 265–322. [https://doi.org/10.1016/0304-4173\(85\)90014-x](https://doi.org/10.1016/0304-4173(85)90014-x)
20. Koopmans, T. (1934). Über die Zuordnung von Wellenfunktionen und Eigenwerten zu den Einzelnen Elektronen Eines Atoms. *Physica I*, 104–113. [https://doi.org/10.1016/s0031-8914\(34\)90011-2](https://doi.org/10.1016/s0031-8914(34)90011-2)
21. Kang, S., & Kim, T. (2020). The nature of electronic and carrier transport properties of M-(quinolate)₂ complexes (M = Be, Mg, Ca, and Sr): A computational study. *Org. Electron.*, 87, 105980. <https://doi.org/10.1016/j.orgel.2020.105980>
22. Liang, Y. et al. (2020). Combined ultrafast spectroscopic and TDDFT theoretical studies on dual fluorescence emissions promoted by ligand-to-metal charge transfer (LMCT) excited states of tungsten-containing organometallic complexes. *Chem. Phys. Lett.*, 748, 137396. <https://doi.org/10.1016/j.cplett.2020.137396>
23. Han, D. et al. (2015). Theoretical design study on the electronic structure and photophysical properties of a series of osmium (II) complexes with different ancillary ligands. *Polyhedron*, 85, 506–510. <https://doi.org/10.1016/j.poly.2014.09.018>.
24. Yadav, R. A. K. et al. (2020). Role of molecular orbital energy levels in OLED Performance. *Sci. Rep.*, 10. <https://doi.org/10.1038/s41598-020-66946-2>
25. Chitpakdee, C. et al. (2014). Theoretical studies on electronic structures and photophysical properties of anthracene derivatives as hole-transporting materials for OLEDs. *Spectrochim. Acta. A Mol. Biomol. Spectrosc.*, 125, 36–45. <https://doi.org/10.1016/j.saa.2013.12.111>
26. Yoshida, H. & Yoshizaki, K. (2015). Electron affinities of organic materials used for organic light-emitting diodes: A low-energy inverse photoemission study. *Org. Electron.*, 20, 24–30. <https://doi.org/10.1016/j.orgel.2015.01.037>
27. Shi, L. L. et al. (2010). Theoretical study on the electron transfer and phosphorescent properties of iridium (III) complexes with 2-phenylpyridyl and 8-hydroxyquinolate ligands. *Dalton Trans.*, 39, 7733–7740. <https://doi.org/10.1039/c0dt00146e>
28. Zou, L. Y. et al. (2011). Theoretical design study on photophysical property of the organoboron quinolate derivatives. *Theor. Chem. Acc.*, 129, 63–71. <https://doi.org/10.1007/s00214-011-0888-x>
29. Chu, T. Y. et al. (2005). Ab initio molecular orbital study of 1,3,5-triazine derivatives for phosphorescent organic light emitting devices. *Chem. Phys. Lett.*, 415, 137–140. <https://doi.org/10.1016/j.cplett.2005.08.149>
30. Kwak, S. W. et al. (2020). Synthesis and photophysical properties of a series of dimeric indium quinolates. *Molecules*, 26, 34. <https://doi.org/10.3390/molecules26010034>
31. Mahmoud, M. E. et al. (2009). Surface layer-by-layer chemical deposition reaction for thin film formation of nano-sized metal 8-hydroxyquinolate complexes. *Polyhedron*, 28, 181–187. <https://doi.org/10.1016/j.poly.2008.09.030>